JOURNAL OF APPLIED ELECTROCHEMISTRY **28** (1998) 1179–1188

Electrochemical processing of porosity gradients for the production of functionally graded materials

A. NEUBRAND

Darmstadt University of Technology, Department of Materials Science, Petersenstrasse 23, 64287 Darmstadt, Germany, E-mail: di1v@hrzpub.tu-darmstadt.de

Received 5 December 1997; accepted in revised form 24 February 1998

The present paper lays the theoretical foundations of a new production process for functionally graded materials (FGMs). The process is based on the evolution of porosity gradients in porous electrodes which undergo electrochemical dissolution or deposition. The electrodes with graded porosity serve as preforms for the production of graded composites by infiltration processing. A one-dimensional macroscopic model of the porous electrode has been used for the prediction of the porosity gradients. A numerical approach allows utilization of experimentally determined current–potential curves for nonporous electrodes, with the incorporation of changes of the pore structure during the course of the electrode reaction, to predict the porosity gradients. For porous copper cathodes and anodes the results of this model are compared with experimentally observed polarization behavior and porosity distributions for different current densities and electrolyte conductivities.

Keywords: *functionally graded materials*, *porous electrodes*, *current distribution*, *infiltration processing*

1. Introduction

Porous electrodes have large active surface areas leading to low current densities at the electrode–electrolyte interface. The use of electrodes with a large active surface allows utilisation of high electrochemical reaction rates per unit volume. This makes the use of porous electrodes very attractive in applied electrochemistry, the most widespread application being the lead–acid battery. Porous electrodes can be used to effectively remove metals or toxic substances from solutions of low concentration [1, 2] and improve the productivity in electrosynthesis processes [3, 4].

Porous electrodes are also the basis of a novel process for the production of so-called functionally graded materials (FGMs), a new class of materials developed in the last decade [5]. FGMs have chemical composition and properties varying continuously with position and may thus be applied in many situations where external loads are unevenly distributed over a component. The gradient can have two different functions: first, it can avoid typical disadvantages of interfaces such as stress concentrations leading to delamination under thermal or mechanical load. In this case the gradient serves to join two materials which are otherwise incompatible; second, a tailored property gradient in FGMs can optimize the response of the component to an external field, a well-known example of such a FGM is glasses with graded refractive index for glass fibres and lenses.

One of the main obstacles towards the practical application of FGMs is the lack of cheap and reliable production processes. Electrochemical processing of FGMs can fulfil these requirements to a large extent for a number of material combinations. In the Electrochemical production process a porous electrode material is either dissolved or deposited electrochemically. The nonuniform current distribution inside the electrode leads to a porosity gradient in the electrode after prolonged operation. Infiltration of the porosity graded electrode with a melt or other liquid precursor of a second material yields a functionally graded material [6]. The method allows the production of FGMs from components with very different melting points which are particularly difficult to produce with more conventional methods like powder processing [7]. Examples are metal–ceramic and metal–polymer FGMs. Electrochemical processing of FGMs allows the production of large quantities of such gradient materials at a reasonable cost. In the present work the evolution of porosity gradients due to nonuniform current distributions in porous copper electrodes has been investigated both theoretically and experimentally. The Cu/Cu^{2+} system was chosen because of its reversible electrode reaction and stable potential.

Knowledge of the current distribution inside porous electrodes is essential for the FGM production process as the shape of the porosity gradient is crucial for most applications. However, the experimental investigation of current distributions is not straightforward. One method is based on the measurement of potential distributions by introducing Luggin capillaries into holes drilled inside the electrodes [8]. The local faradaic current can then be calculated from the

0021-891X

second derivative of the potential using (4). This method requires knowledge of the electrochemically active surface area and the effective conductivity of the electrolyte in the pore system. Furthermore, small errors in the measurement of potential or position cause large errors in the current distribution. Current distributions have also been determined by radiographic methods using radioactive tracers [9], but the method has only limited spatial resolution and calibration is not straightforward. It is also possible to weigh the deposit on a sectioned porous electrode in order to determine current density distributions [10]. In this paper a related method has been used, the amount of material removed or deposited was determined by image analysis of micrographs. The spatial porosity profile observed is directly related to the current distribution in the electrode. In the present work, experimentally observed porosity distributions and potentials in porous copper electrodes are compared to theoretical ones. It will be shown that a prediction of the potential and current distribution over a wide range of operating conditions requires a numerical solution of the underlying differential equations and the use of experimentally determined current potential curves for flat electrode surfaces.

2. Theory

The problem of current density distribution in porous electrodes is important for their effective use in many processes, and therefore this problem has been addressed in a number of theoretical publications for a variety of operating conditions and electrode configurations [11–19]. Comprehensive treatments of this topic have been published by Roušar *et al*. and Levie [20, 21]. In this work a continuum model is used which considers the porous electrode as a solid solution or a macrohomogenous mixture of two continuous phases, that is, the electrode matrix and the electrolyte filling the pores. This implies that the electrode is much larger than the particles and pores composing it and the electric double layer is small compared to the pore dimensions. It is assumed that concentration gradients inside the porous electrode can be neglected and the current in the cell is charge-transfer limited. These assumptions hold well at low to moderate current densities for flow-through porous electrodes with high flow rates as were encountered in the experiments performed in the course of this work.

2.1. *Analytical calculation of current distribution*

Let us consider a porous anode with anode reaction

$$\mathrm{M}(s) \rightarrow \mathrm{M}^{z}(\mathrm{aq}) + z\mathrm{e}^{-} \tag{1}$$

where M(s) is the porous anode material and $\mathrm{M}^{z+}(\mathrm{aq})$ is a soluble product. The following calculations can be carried out for cathodes in a similar manner by replacing anodic by cathodic processes. During operation of a porous electrode, potential gradients occur in the liquid phase, and for electrode materials with moderate conductivity, also in the solid phase. These potential gradients can be calculated from the current density in the solid phase (j_s) and liquid phase (j_l) by Ohm's law:

$$\vec{j}_{\mathrm{s,l}} = \frac{1}{\rho^*_{\mathrm{s,l}}} \nabla \varphi_{s,l} \tag{2}$$

where $\varphi_{\mathrm{s,l}}$ are the potentials of the electrode and the electrolyte, respectively, ∇ is the Nabla operator. ρ^*_s is the effective resistivity of the porous electrode and ρ^*_l the effective resistivity of the electrolyte inside the percolating pores that is, the resistance of the electrolyte filling a cube of the porous electrode of unit dimensions. ρ^*_s and ρ^*_l are related to the porosity P of the electrode by

$$\rho^*_\mathrm{s} = \rho_\mathrm{s} \frac{u_\mathrm{s}}{(1-P)} \tag{3a}$$

and

$$\rho^*_\mathrm{l} = \rho_\mathrm{l} \frac{u_\mathrm{l}}{P} \tag{3b}$$

where ρ_s and ρ_l are the bulk resistivity of the solid (s) and the electrolyte (l), respectively. The tortuosity factors u_l and u_s describe the increase in resistivity due to the curvature and constriction of the pores or solid microstructural elements. Typical values for u_s and u_l are 2–7 [22].

Consider a plate-like porous anode of thickness L where the current feeder is located at the side opposite to the cathode (Fig. 1). From Ohm's law (Equation 2) and the condition of electroneutrality, the following one-dimension differential equation can be derived (neglecting transient response effects) [17]:

$$\frac{\mathrm{d}^2}{\mathrm{d}x^2}\eta = S j_\mathrm{F}(\rho^*_\mathrm{l} + \rho^*_\mathrm{s}) \tag{4}$$

where η is the overpotential, j_F is the local faradaic current density per unit internal surface are, and S is the specific surface area per unit volume. The boundary conditions result from the fact that the total current j_T in the anode is purely electronic at $x = 0$ (i.e., $j_\mathrm{l}(0) = 0,\ j_\mathrm{s}(0) = j_\mathrm{T}$) while the current is purely ionic at $x = L$, that is, $j_\mathrm{l}(L) = j_\mathrm{T},\ j_\mathrm{s}(L) = 0$ at the face close to the cathode. Using Ohm's law (Equation 2) and the definition of overpotential:

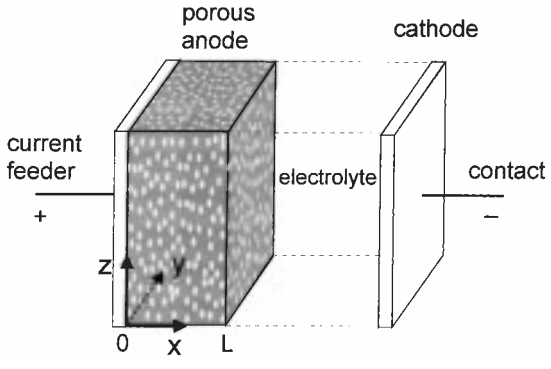

Fig. 1. Geometry of porous electrode.

$$\frac{\mathrm{d}}{\mathrm{d}x}\eta = -j_s\rho_s^* + j_l\rho_l^* \tag{5}$$

Using Equation 5 the boundary conditions can be expressed in the more convenient form

$$\frac{\mathrm{d}}{\mathrm{d}x}\eta(0) = -j_T\rho_s^* \tag{6}$$

$$\frac{\mathrm{d}}{\mathrm{d}x}\eta(0) = j_T\rho_l^* \tag{7}$$

Using these boundary conditions Equation 4 can now be solved for different current potential relations $j_F(\eta)$.

2.1.1. Solution for large electrode polarization. In the case of high overpotential, the Tafel relation can be used to describe the dependence of faradaic current on overpotential:

$$j_F(\eta) = j_0 \exp\left(\frac{\alpha F}{RT}\eta\right) \tag{8}$$

where j_0 is the exchange current density and α the transfer coefficient of the electrode reaction. After the introduction of Equation 8 into Equation 4 the solution of the differential equation becomes:

$$\eta(w) = \frac{RT}{\alpha F}\ln\left[\frac{B}{2A}\left\{1 + \mathrm{tg}^2\left([w - w_{\min}]\frac{\sqrt{B}}{2}\right)\right\}\right] \tag{9}$$

where the relative position $w = x/L$ has been introduced. A and B are dimensionless constants defined by the following equations:

$$A = (\rho_l^* + \rho_s^*)L^2 S j_0 \frac{\alpha F}{RT} \tag{10}$$

$$\mathrm{arc\,tg}\left(\frac{C}{\sqrt{B}}\right) + \mathrm{arc\,tg}\left(\frac{D}{\sqrt{B}}\right) = \frac{\sqrt{B}}{2} \tag{11}$$

with

$$C = \rho_s^* j_T L \frac{\alpha F}{RT} \quad \text{and} \quad D = \rho_l^* j_T L \frac{\alpha F}{RT} \tag{12}$$

where j_T is the total current density, that is the current per unit of projected geometric area of the porous electrode. The position of minimum overpotential is determined by the dimensionless quantity $w_{\min}$:

$$w_{\min} = \left(\frac{2}{\sqrt{B}}\right)\mathrm{arc\,tg}\left(\frac{C}{\sqrt{B}}\right) \tag{13}$$

From Equation 9 the local current density per unit volume j_v is obtained:

$$j_v = S j_F = j_0 S \frac{B}{2A}\left\{1 + \mathrm{tg}^2\left([w - w_{\min}]\frac{\sqrt{B}}{2}\right)\right\} \tag{14}$$

2.1.2. Solution for low electrode polarization. In the case of low electrode polarization the faradaic current is proportional to overpotential η:

$$j_F = j_0 \frac{\alpha F}{RT}\eta \tag{15}$$

where α is an experimentally determined constant (note that even for the same electrode reaction, α will usually not have the same value as that used in Equation 8). Inserting Equation 15 into Equation 4 and solving the resulting differential equation yields

$$\eta(w) = \frac{j_T L}{\sqrt{A}\sinh(\sqrt{A})}\{\rho_s^* \cosh[\sqrt{A}\,(w-1)] + \rho_l^* \cosh(\sqrt{A}\,w)\} \tag{16}$$

From Equation 16 the local current density per unit volume can be determined

$$j_v = j_T\sqrt{\frac{j_0 S}{\rho_s^* + \rho_l^*}\left(\frac{\alpha F}{RT}\right)} \times \frac{\{\rho_s^* \cosh[\sqrt{A}\,(w-1)] + \rho_l^* \cosh[\sqrt{A}\,w]\}}{\sinh(\sqrt{A})} \tag{17}$$

It is noteworthy that the shape of the current distribution inside the porous electrode depends only on the parameter $\sqrt{A}$ which can be regarded as the inverse of a relative penetration depth. Hence, for the production of a porosity gradient that extends over most of the electrode, the experimental conditions should be chosen such that A is on the order of unity. The current distribution is independent of the total applied current j_T, but becomes more homogeneous with decreasing exchange current density, transfer coefficient, specific surface area and resistivity of the liquid and solid phase.

2.2. *Numerical simulation*

The analytical given above are valid for the idealized current–potential curves. In reality the dependence of current on electrode polarization may be more complex and an analytical solution for the current distribution is, in general, not available. To be able to use experimentally determined current–potential curves, a numerical model based on the same equations as the analytic solution has been developed.

In the present work, a one dimensional flat electrode was modelled using an iterative finite difference scheme. For this purpose, the electrode was divided into n elements of equal size (Fig. 2). Each element has an electrolyte part and an electrode part representing the attributes of the pore and the solid at the

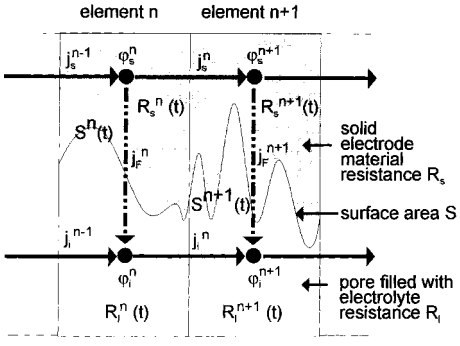

Fig. 2. Two elements of the numerical model and their properties.

specific position and time. The elements are homogenous in porosity, specific surface area, resistance and all other properties. Assuming galvanostatic or potentiostatic control and using the same boundary conditions as in the analytical model, the potential development from one element to the next can be calculated regarding the elements as a network of resistances and calculating the faradaic current for each element separately. Starting values for the potential (galvanostatic case) or current (potentiostatic case) were taken from analytical approximations. The algorithm is sketched in Fig. 3. The potential (galvanostatic case) or the current (potentiostatic case) is varied in subsequent iterations until the boundary conditions are fulfilled.

For larger mass losses various parameters associated with the pore structure (e.g. specific surface area) will change during cell operation. The mass loss depends not only on the duration of electrolysis but also on position. A position dependent porosity, specific surface area and tortuosity will develop during the experiment. All these parameters influence the potential and current distribution during the dissolution process. For the calculations in Section 4.3, a dependence of the effective electrolyte and electrode conductivity on porosity P according to Equation 3 was used. The tortuosity factors were assumed to be independent of P. Experimentally determined functions $S = S(P)$ were used for the dependence of specific surface area on porosity. The changes of these properties were included in the numerical model in the following way: The initial current distribution was calculated. From this the density change after a time interval of 1/500 of the total experiment duration was computed. Using the altered porosity distribution a new current distribution was calculated and the resulting porosity changes in this second time interval were added to those of the first time interval. This procedure was repeated until the total time of the experiment was reached.

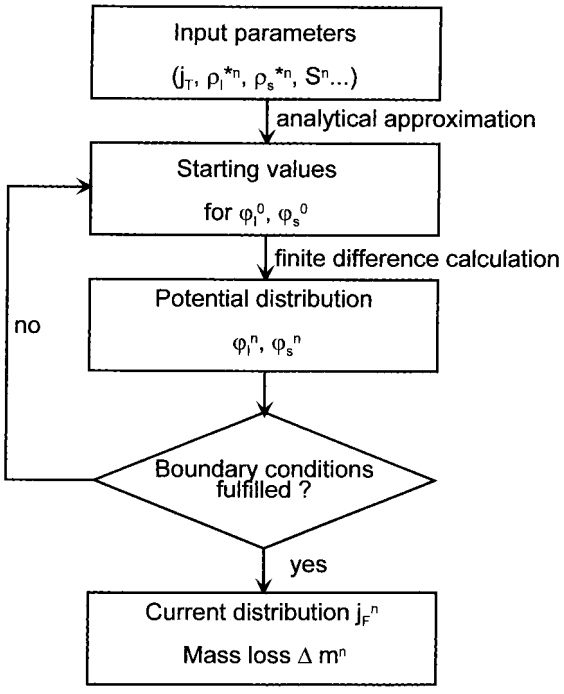

Fig. 3. Flow chart of the numerical algorithm.

3. Experimental details

Porous, sintered copper was used as a porous electrode material in the electrochemical cell. The basic properties of the porous electrode are listed in Table 1. The initial average porosity of the copper electrodes was determined by weighing and was between 40% and 46% for all specimens. The tortuosity factor of the pore system was not measured, but a value determined for porous tungsten electrodes of the same porosity and similar microstructure was used. The electrodes were fixed in silicon rubber and their back was connected as working electrode to a galvanostat. This prevented penetration of the electric field from the side into the sample. A copper-plated platinum counter electrode of 30 mm × 30 mm area was mounted parallel to the porous electrode at a distance of about 10 mm.

Prior to the experiment the porous electrode was evacuated and completely infiltrated with the electrolyte. The electrolyte consisted of reagent grade 0.1 M $CuSO_4$ and H_2SO_4. The conductivity of the electrolyte was varied by adding different amounts of H_2SO_4. It was measured at the beginning and the end of the experiment, with only negligible changes observed. A pump connected to the bottom of the anode provided a continuous flow of electrolyte of 120 ml min^{-1} through the porous electrode maintaining the electrolyte concentration inside the pore network almost constant.

All experiments were carried out in a galvanostatic mode. For the potential measurements a Luggin capillary was placed as close as possible to the front of the electrode and the current was increased to a maximum value and then decreased again while the potential was recorded. To determine the current distribution in the electrodes, the cell was operated for longer time intervals. The total amount of charge passed through the electrode was between 500 and 1000 C cm^{-2} of outer electrode surface within 25 to 100 h. This caused significant amounts of copper to be deposited or dissolved. After electrolysis the samples were flushed several times with demineralized water and dried in order to remove the electrolyte. To determine the amount of copper deposited or dissolved at different positions the copper electrodes

Table 1. Initial properties of copper electrodes

Property	*Value*
Porosity	43%
Specific surface area per volume	8030 m^{-1}
Tortuosity factor of the pore system	3.5
Dimensions	30 mm × 30 mm × 3 mm

were embedded in fluorescent epoxy resin. Slices were cut parallel to the porosity gradient and the sections were ground and polished. An optical microscope with an image analysing system (Quantimet, Leica Germany) was employed for the quantitative determination of the copper content and the specific surface area per unit volume as a function of position. At least 10 measurements perpendicular to the concentration gradient were carried out to reduce the error due to inhomogeneities of the microstructure.

4. Results and discussion

4.1. *Polarization of nonporous copper electrodes*

To obtain basic information about the polarization behaviour of copper the current potential curves of a nonporous copper electrode in a solution containing 0.1 M $CuSO_4$ and 0.6 M H_2SO_4 were determined (Fig. 4). A Butler–Volmer type of equation

$$j_F = j_0\left(\exp\frac{\alpha_a F\eta}{RT} - \exp\frac{-\alpha_c F\eta}{RT}\right) \qquad (18)$$

can be used to describe the relationship between current density and overpotential for a two electron reaction if one reaction step is rate controlling [23]. The experimental data was fitted using an anodic transfer coefficient of 1.02, a cathodic transfer coefficient of 0.58 and exchange current density of 3.5 A m^{-2} (thick solid curve). These values were used for all the calculations reported here. The cathodic transfer coefficient compares well with values reported in the literature which are in the range of 0.42–0.62 [23]. However, the anodic transfer coefficient determined is lower than the values of 1.18–1.51 reported earlier. The difference can be attributed to the fact that in this work the whole polarization curve, including the low polarization part, has been fitted using three constants (two transfer coefficients and one exchange current density), whereas transfer coefficients in the literature were determined evaluating the Tafel slope; this means a fit of only the high polarization part with transfer coefficient and exchange current density each for positive and negative polarization. Indeed, evaluation of experimental values at overpotentials above 30 mV with the latter method yields a transfer coefficient of 1.32 and an exchange current density of 1.7 A m^{-2}. The discrepancy is therefore caused by the type of evaluation. For our purpose, that is, for the calculation of the current and potential in porous electrodes, it was decided that the method with three constants is more appropriate as it makes use of the experimental values determined at low polarization. Proper description of the current density values at low potentials was regarded as particularly important as a large part of the porous electrode was at overpotentials below 30 mV in the experiments. Also shown in the plot is a polarization curve employing the linear relation (Equation 15) with the same parameters for α_a, α_c and j_0 as given above (thin solid curve). At overpotentials below 20 mV the linear relation is suitable to describe the polarization behaviour of copper electrodes. For comparison the two Tafel lines are also plotted (dashed line in Fig. 4). The Tafel lines fit the experimental values for potentials above 40 mV.

4.2. *Polarization of porous copper electrodes*

The potential at the front side of the porous electrode as a function of current was determined in a series of experiments to check the predictions made by the models mentioned above. The polarization of a porous copper anode in an electrolyte containing 0.1 M $CuSO_4$ and conductivity of 330 mS cm^{-1} is shown in Fig. 5. Also shown are the theoretical predictions for

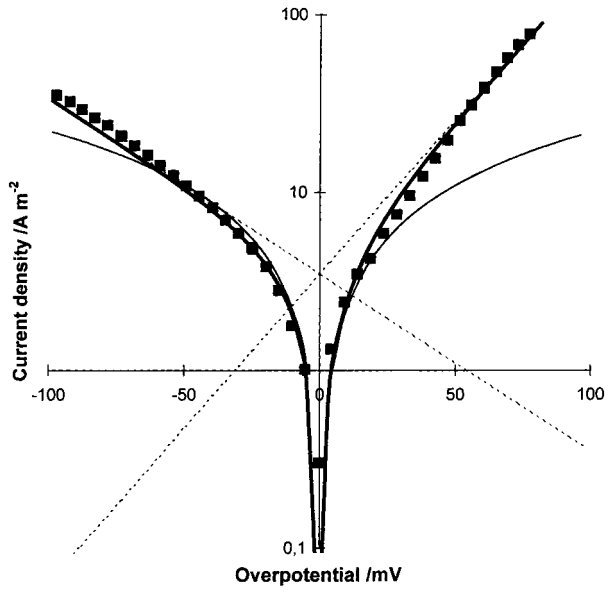

Fig. 4. Tafel plot for a nonporous copper electrode in 0.1 M $CuSO_4$. Key: (■) experimental data; (—) fit with Butler–Volmer equation; (—) linear fit; (----) Tafel line.

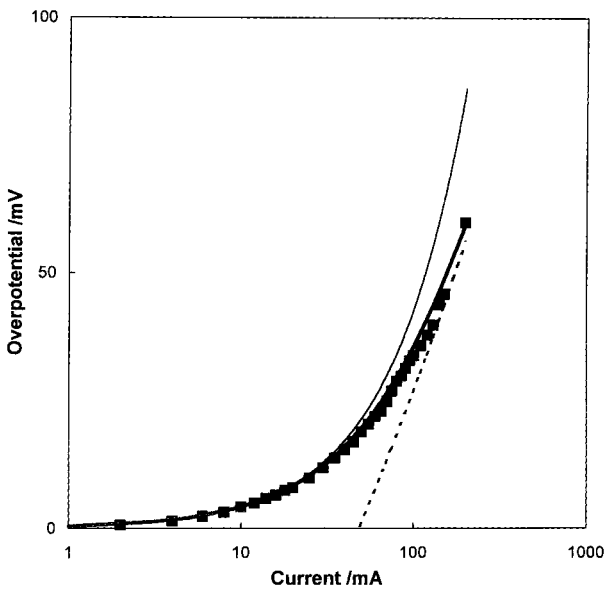

Fig. 5. Polarization of a porous copper anode in 0.1 M $CuSO_4$. Key: (■) experiment; (—) Butler–Volmer; (—) linear; (----) exponential model.

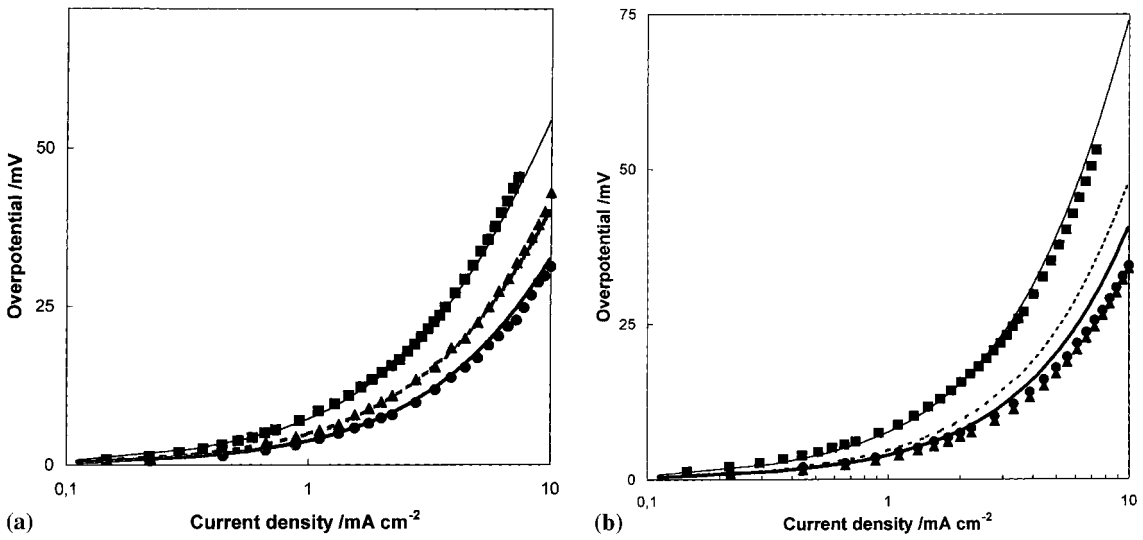

Fig. 6. Polarization of a porous copper electrode in electrolytes of variable conductivity. (a) Anode, experimental values: (■) 80, (▲) 187 and (●) 330 mS cm^{-1}; theory: (—) 80, (----) 187 and (—) 330 mS cm^{-1}. (b) Cathode, experimental values: (■) 80, (▲) 221 and (●) 330 mS cm^{-1}; theory: (—) 80, (----) 221 and (—) 330 mS cm^{-1}.

the polarization curve using the aforementioned three different assumptions for the current potential dependence. It is evident that under the experimental conditions neither a linear nor an exponential dependence of current on potential was able to predict the polarization of the porous electrode in the full overpotential range from 0 to 60 mV. This is not surprising as the behaviour of the nonporous electrode could not be described in this potential range by either of these simplified current potential functions. The numerical solution employing the Butler–Volmer equation was, however, able to predict the polarization of the electrode in the full range of potentials studied. The difference between the measured and the predicted polarization is comparable to that of the nonporous electrode (Fig. 4). Figure 6(a) shows the anodic current–potential curves for three different electrolyte conductivities. It is obvious that the polarization decreases with increasing conductivity of the electrolyte. This can be explained qualitatively by the fact that electrolytes with high conductivity cause a smaller potential drop inside the porous electrode; therefore, a larger volume of the electrode is used for the electrode reaction leading to a smaller polarization. The theoretical prediction of the electrode polarization is in good agreement for all three electrolytes. The same type of measurement was also performed for cathodic polarization (Fig. 6(b)). The same trends are visible, and the agreement with theory is still reasonable, but the predicted overpotentials tend to be higher than the observed values. The disagreement between the theoretical and experimental curve is slightly larger than in Fig. 4. One reason may be small differences in the pore structure from electrode to electrode, which have a marked effect on the current potential curve.

4.3. *Porosity distribution inside porous copper electrodes*

The porosity distribution inside the porous electrodes developed after their operation is the most crucial property in the production process for FGMs. Therefore, the amount of copper deposited or dissolved at different position of the porous electrode was determined by image analysis. The average current density distribution during the experiment can be determined from the electrode density using the parameters of the experiment (Table 2).

The error bars in the displayed porosity distributions result from a statistical analysis, systematic errors caused by the sample preparation and variations in the initial porosity of the electrode are not included. Inspection of electrodes before the electro-

Table 2. Experimental parameters for samples A–G

Sample	*Type*	*Total charge* /C cm^{-2}	*Total c.d.* /mA cm^{-2}	*Electrolyte cond.* /mS cm^{-1}
A	cathode	500	2.77	221
B	anode	1000	5.55	164
C	cathode	500	5.55	221
D	anode	1000	2.77	221
E	anode	1000	5.55	221
F	cathode	500	5.55	80
G	anode	1000	5.55	330

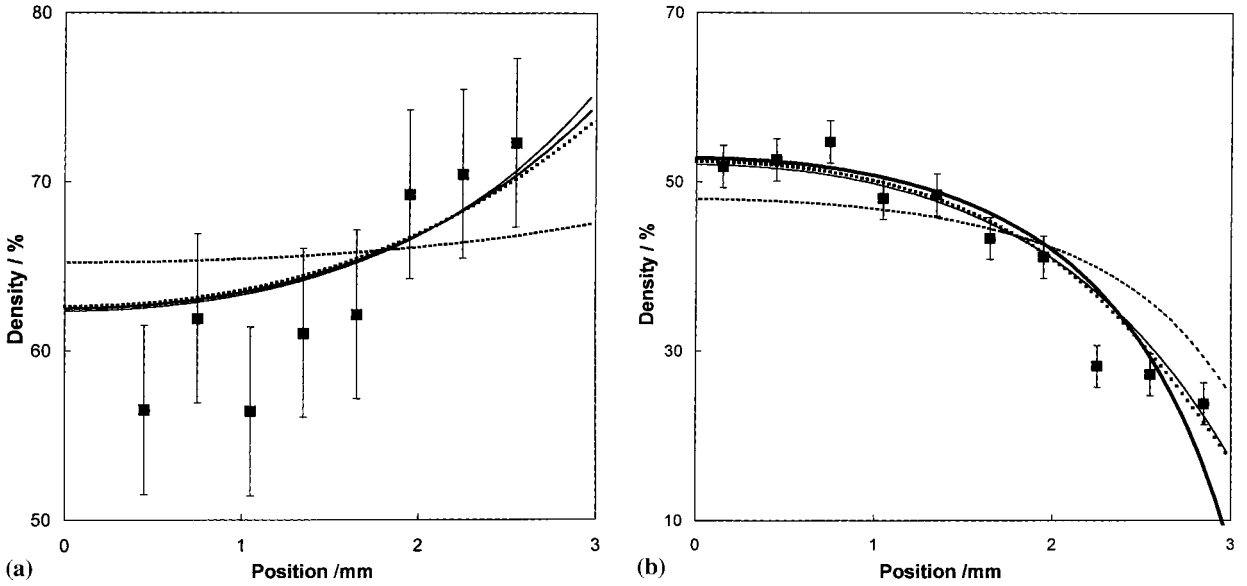

Fig. 7. Experimental and theoretical density distribution in porous copper electrodes. (a) Cathode (sample A), (b) anode (sample B). Key: (■) experimental values; (—) linear; (----) exponential; (—) Butler–Volmer; (···) time-dependent model.

chemical gradation showed global initial porosity variations of up to 6% in different samples and local variations within samples of up to 8% .

4.3.1. Observed and predicted porosity distributions. The observed density distribution in a porous copper cathode (sample A, cf. Table 2) is shown in Fig. 7(a) together with the predictions of the aforementioned models. The following models were used to calculate the current distribution. The two models for linear (Equation 15) and exponential (Equation 8) current potential relationships, and a numerical model using the Butler–Volmer equation (18). For simplicity these will be called the linear, exponential and Butler–Volmer models. The density change was calculated assuming a current yield of 100% and the current distribution to be independent of time (the first assumption holds for the copper system, the second assumption will be discussed later in detail). The exponential model obviously does not describe the experimental data. This could be expected as most of the electrode was at low potentials where Equation 8 is not valid. In contrast, at low potentials the linear approximation of the Butler–Volmer relation is applicable: this is why both the linear and the Butler–Volmer model give a reasonable fit of the experimental data.

In the course of the galvanostatic experiments overpotential changes of up to 15 mV were observed (the rest potential was not altered). These changes are caused by the changing surface area and porosity of the electrode, which may in turn affect the porosity gradient developed. Therefore, in many situations such porosity changes cannot be neglected, especially in the production process for gradient materials where the evolution of large porosity differences in the electrode are the purpose of the cell operation. Fig. 7(b) shows such a case (sample B), the maximum density variation is more than 30% . In order to account for the changing pore structure quantitatively the change of the specific surface area with porosity was determined for all electrochemically altered porous electrodes by optical microscopy. The determined data points are shown in Fig. 8 together with a fit of the experimental values with a polynomial function of fourth order. Using this fit and assuming a linear dependence of the effective conductivity of the electrolyte on porosity the density distribution was calculated using a Butler–Volmer current potential relationship (time-dependent model in Fig. 7(a) and 7(b)). This model predicts the porosity evolution very well for sample B: only the linear model yields a

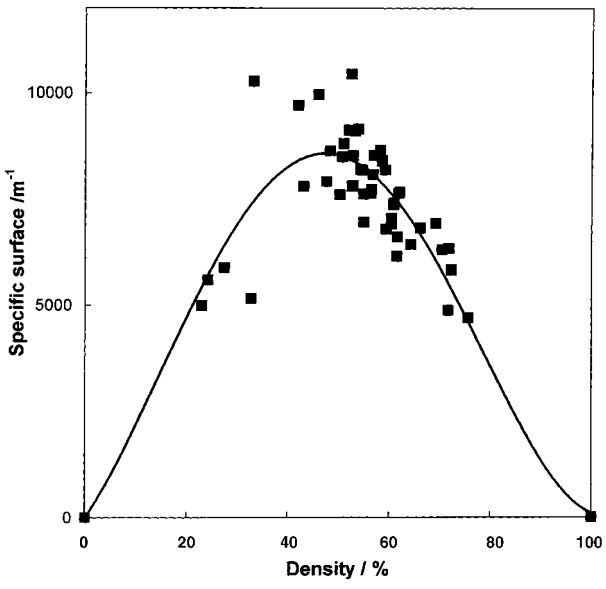

Fig. 8. Specific surface area per unit volume as a function of density for a porous copper electrode. Squares represent experimental data, the line is a fit with a 4th order polynomial.

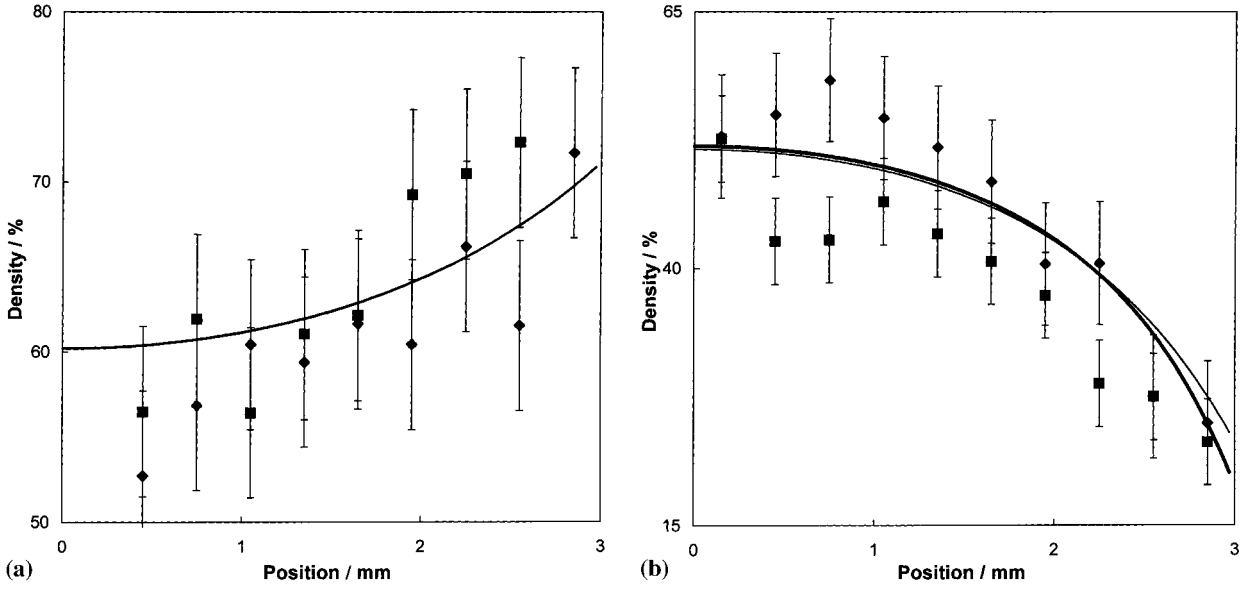

Fig. 9. Density distributions for porous copper electrodes with different current densities. (a) Cathode: (■) 2.77 (sample A); (◆) 5.55 mA cm^{-2} (sample C); (—) theory (sample A and C). (b) Anode: (■) 2.77 (sample D); (◆) 5.55 mA cm^{-2} (sample E); (—) theory (sample D); (—) theory (sample E).

comparable fit of the experimental data, however, without having a similarly sound physical basis. Using a time-dependent pore structure for a linear current potential relationship did not result in a good fit of the experimental data; it is therefore concluded that the agreement with the linear model is coincidental. The decreasing surface area and increasing porosity in the front portion of the porous anode both flatten the current distribution which explains why the time-independent Butler–Volmer model overestimates the density change.

The changes to the pore structure affect the modelling results much less for sample A (Fig. 7(a)). The reasons are the following: first, the overall change in porosity is lower due to the lower total charge passed through the electrode, which makes the effect less pronounced; second, for electrodeposition both the surface area and conductivity decrease. The decreasing surface area in the front portion of the electrode leads to a flattened current distribution whereas the narrowing of the pores leads to a decreasing effective electrolyte conductivity and a steeper current distribution. As a result the two effects partially cancel each other and the effects of pore narrowing on current distribution is less pronounced for sample A. Obviously a proper description of the porosity changes must take into account effects of changing pore structure and therefore in the following density distribution, only the results of the time-dependent model employing the Butler–Volmer relation are reproduced.

4.3.2. Dependence of the density distribution on total current density. In a series of experiments the dependence of the density (and thus current density) distribution on the applied total current density was determined. For low electrode polarization the linear approximation holds, which predicts that the relative current distribution does not depend on total current density. This is confirmed by Fig. 9(a) which shows the density change of a porous cathode at total current density of 2.77 and 5.55 mA cm^{-2} where the total amount of charge was kept constant at 500 C cm^{-2} (samples A and C). No clear differences in the density distributions are visible, the slightly higher density values of sample A are probably due to a slightly decreased initial porosity as compared to sample C. The differences in the predicted density distributions are so small for both samples that they are represented by one line in the plot. Fig. 9(a) proves that the current distribution does not depend on the total current density at small overpotentials. The result for a porous anode and identical conditions (samples D and E) are shown in Fig. 9(b). The experimental density values for sample D (2.77 mA cm^{-2}) are generally about 5% lower than predicted, this is probably due to a lower initial density of this sample. The current distribution at 2.77 mA cm^{-2} appears to be more homogeneous than at 5.55 mA cm^{-2}, although the difference is within the order of the experimental errors. Indeed, the theory predicts a small difference in this case with a more inhomogeneous current distribution at higher total current. The different current distributions for the cathodic and anodic process can be explained by the higher transfer coefficient for the anodic reaction: this means that the nonlinear regime of current potential dependence is reached at lower potentials and the current distribution starts to depend on the total current density. This fact is further supported by Fig. 10 where the dependence of density distribution is plotted for a porous tungsten anode dissolved in sodium hydroxide solution. Due to the lower exchange current density for this reaction the applied overpotentials were several hundred millivolt and thus the exponential model should hold, which predicts a strong

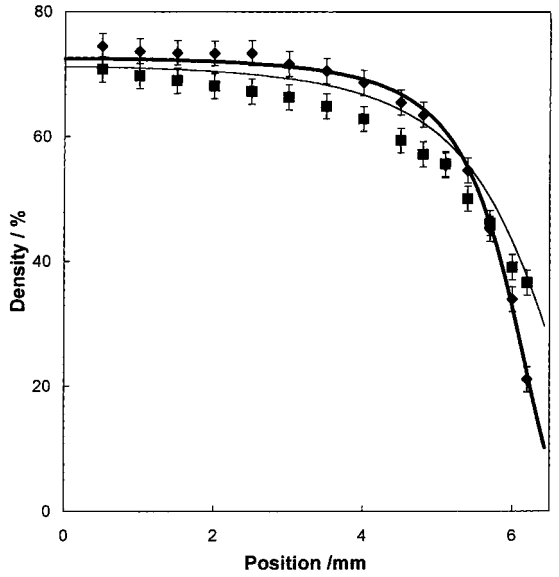

Fig. 10. Density distributions for a porous tungsten anode with different current densities: (■) 5.5, (◆) 12.2, (—) theory 5.5 and (—) theory 12.2 mA cm^{-2}.

dependence of density distribution on current. This is indeed observed with the density (and current) distribution much more inhomogeneous for the higher total current density.

4.3.3. Dependence of the density distribution on the effective electrolyte conductivity. Figure 11(a) shows the dependence of the density distribution which developed in a porous copper cathode for two different electrolytes of 80 and 221 mS cm^{-1} conductivity (samples F and C). It is clear that the distribution is almost homogeneous for the highly conductive electrolyte and inhomogeneous for the less conductive electrolyte. This agrees well with calculations of the density distribution which predict a strong dependence on the effective electrolyte conductivity in the pore system for low and high overpotential.

Figure 11(b) shows the dependence of the density distribution for porous copper anodes dissolved in an electrolyte with 164 and 330 mS cm^{-1} conductivity (samples B and G). Again it can be recognized that the density distribution becomes more inhomogeneous with decreasing effective conductivity of the electrolyte in the pores. The theoretical prediction again fits the experimental data reasonably.

5. Conclusions

The polarization and current distribution in flow-through porous electrodes has been determined both experimentally and theoretically for low and medium overpotential. A continuum model of the electrode has been used to describe the polarization and the current distribution at the beginning of cell operation.

The predictions of the theory of flow-through porous electrodes at constant concentrations could be verified experimentally for anodic and cathodic polarization:

(a) The current distribution is independent of the total current density at low overpotential. At high overpotential the current distribution becomes more inhomogeneous with increasing current density.
(b) The current distribution becomes more inhomogeneous with decreasing effective conductivity of the electrolyte and electrode at low and high overpotential. Usually the conductivity of the electrolyte is much lower than that of the electrode and controls the current distribution.

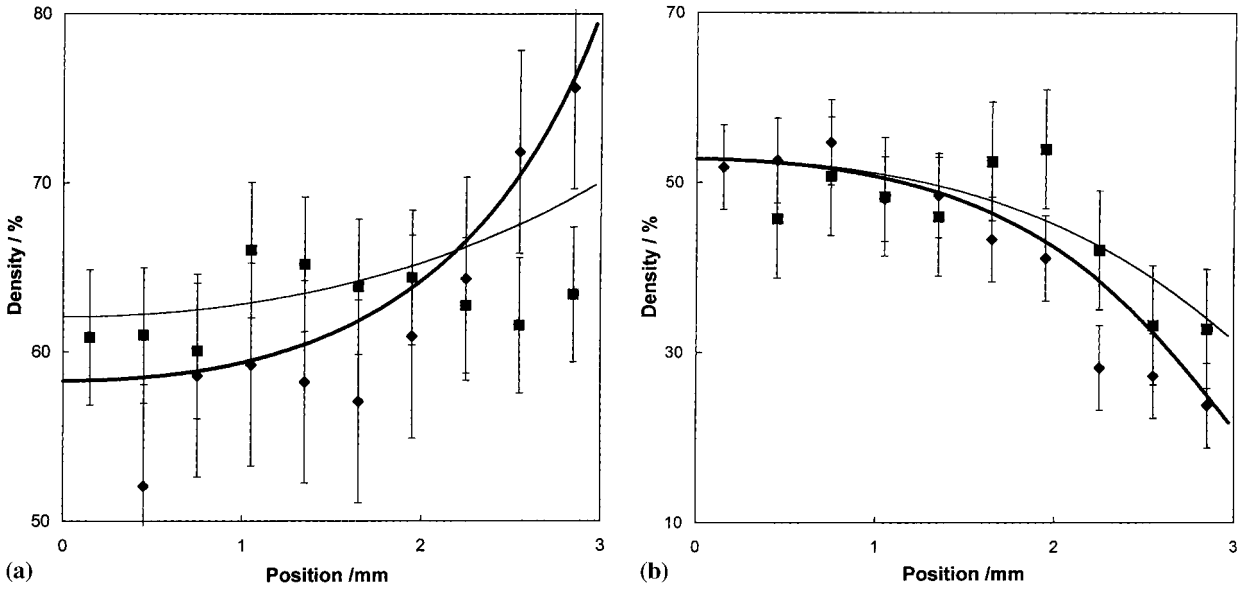

Fig. 11. Density distributions for a porous copper electrodes with different electrolyte conductivities. (a) Cathode: (■) 221 (sample C), (◆) 80 (sample F), (—) theory 221, (—) theory 80 mS cm^{-1} (sample F). (b) Anode: (■) 330, (sample G), (◆) 164 (sample B), (—) theory 330 and (—) theory 164 mS cm^{-1}.

This implies that a higher porosity will lead to a more evenly distributed current.

If the electrode material itself takes part in the electrode reaction, the current distribution changes at prolonged cell operation due to the modification of the pore structure. A finite difference method has been used successfully to calculate the effects of the altered pore structure on current distribution. A precise prediction of the porosity gradient developed during the anodic dissolution of porous electrodes appears viable if the parameters of the electrochemical reaction and the porous structure are precisely known. This is crucial for the electrochemical processing of functionally graded materials. The electrochemical method presented here thus appears to be attractive for predictable and cost-effective processing of preforms for functionally graded materials.

Acknowledgements

I am indebted to R. Jedamzik for assistance in preparing the manuscript and to Prof. H. Wendt, Darmstadt for carefully reading it. Support of this work by the German Research Society is gratefully acknowledged.

References

[1] J. M. Marrocino, F. Coeuret and S. Langlois, *Electrochim. Acta* **32** (1987) 1303.
[2] T. Doherty, J. G. Sunderland, E. P. L. Roberts and D. J. Pickett, *ibid.* **41** (1996) 519.
[3] J. R. Backhurst, J. M. Coulson, F. Goodridge, R. E. Plimley and M. Fleischmann, *J. Electrochem. Soc.* **116** (1969) 1600.
[4] C. J. Brown, D. Pletcher, F.C. Walsh, J. K. Hammond and D. Robinson, *J. Appl. Electrochem.* **24** (1994) 95.
[5] A. Neubrand and J. Rödel, *Z. Metallk.* **88** (1997) 358.
[6] R. Jedamzik, A. Neubrand and J. Rödel, submitted to *J. Mater. Sci.*
[7] A. Mortensen and S. Suresh, *Internat. Mater. Rev.* **40** (1995) 239.
[8] V. S Daniel-Bekh, *J. Phys. Chem.* (*Russian*) **22** (1948) 697.
[9] K. J. Euler, *ETZ-A Germany* **91** (1970) H11.
[10] R. C. Alkire and B. Gracon, *J. Electrochem. Soc.* **122** (1975) 1594
[11] J. Newman and C. W. Tobias, *ibid.* **109** (1962) 1183
[12] A. Winsel, *Z. Electrochem.* **66** (1962) 287.
[13] E. A. Greens II and C. W. Tobias, *Ber. Bunsenges. Phys. Chem.* **68** (1964) 236.
[14] I. G. Gurevich and V. S. Bagotzky, *Electrochim. Acta* **9** (1964) 1151.
[15] I. G. Gurevich and V. S. Bagotzky, *ibid.* **9** (1967) 593.
[16] R. C. Alkire, E. A. Greens II and C. W. Tobias, *J. Electrochem. Soc.* **116** (1969) 1328.
[17] R. E. Sioda, *Electrochim. Acta* **16** (1971) 1569.
[18] S. Langlois and F. Coeuret, *J. Appl. Electrochem.* **20** (1990) 740.
[19] A. Storck, M. A. Enriquez-Granados, M. Roger and F. Coeuret, *Electrochim. Acta* **27** (1982) 293.
[20] I. Roušar, K. Micka and A. Kimla, 'Electrochemical Engineering, Chemical Engineering Monographs', Vol. 21B, Elsevier, Amsterdam (1986).
[21] R. de Levie, *in* 'Advances in Electrochemistry and Electrochemical Engineering', Vol 6, (edited by P. Delahay), Interscience, New York (1967).
[22] F. A. L. Dullien, 'Porous Media; Fluid Transport and Pore Structure', 2nd edn., Academic Press, CA. (1992)
[23] A. R. Despic, *in* 'Comprehensive Treatise of Electrochemistry', Vol. 7 'Kinetics and Mechanisms of electrode processes', B. E.Conway, J. O. M. (edited by Bockris, E. Yeager, S. U. M. Khan, R. E. White) Plenum, New York (1983).